https://doi.org/10.1016/j.jpowsour.2021.230023

A computational model of a liquid e-fuel cell

Oladapo Christopher Esan[#,1], Xingyi Shi[#,1], Xiangyu Su[1], Yichen Dai[1], Liang An*[,1], T.S. Zhao*[,2]

[1] Department of Mechanical Engineering, The Hong Kong Polytechnic University, Hung Hom, Kowloon, Hong Kong SAR, China

[2] Department of Mechanical and Aerospace Engineering, The Hong Kong University of Science and Technology, Clear Water Bay, Kowloon, Hong Kong SAR, China

[#] These authors contributed equally to this work.

* Corresponding authors.

Email: liang.an@polyu.edu.hk (L. An)

Email: metzhao@ust.hk (T.S. Zhao)

Abstract

A new energy storage system that utilizes electrically rechargeable liquid fuels (e-fuels) obtainable from diverse electroactive materials has been recently proposed. The system is composed of an *e-fuel charger* to charge e-fuels and an *e-fuel cell* to generate electricity for end use. Here, we develop a model for a liquid *e-fuel cell* by incorporating fluid flow and mass/charge transport processes coupled with electrochemical reactions of the involved electroactive species. The mathematical model is validated against the experimental data in the open literature. The model allows to study the effects of various operation variables, including e-fuel concentration, sulfuric acid concentration, e-fuel flow rates, as well as structural design parameters, including the anode porosity and thickness, the membrane and cathode catalyst layer thickness, on the cell performance. The

simulation results reveal that the cell performance improves with increasing e-fuel concentration, sulfuric acid concentration, and e-fuel flow rate. As for the aforementioned structural design parameters, the cell performance increases with increasing these parameters except the membrane thickness where performance degradation is found. The model also reveals that the performance of the e-fuel cell improves with an increase in both anodic and cathodic exchange current densities due to reduced overpotentials. This study therefore provides insights into the performance-enhancing and performance-limiting parameters, as well as design optimization of the liquid *e-fuel cell*.

Keywords: E-fuel; fuel cells; liquid e-fuel cells; computational modeling; mass transport; cell performance

1. Introduction

The quest for carbon-neutral energy options, in lieu of the inefficient and exhaustible conventional energy sources, has stimulated and accelerated the utilization of renewables as promising alternative to match up with the ever-increasing energy demands of the modern world [1-3]. Consequently, several electrochemical energy storage systems have been developed, explored, and deployed not only to supply reliable power, but to also store excess energy gleaned from the sporadic renewable energy sources [4-7]. To attain long-term storage of the garnered electrical energy, the conversion of electricity to fuels for storage has been identified as one of the most promising pathways. This therefore leads to the introduction and embracement of hydrogen fuel cells for diverse energy-related applications including electric vehicles [8-12]. Safety and energy efficiency concerns among other limitations of utilizing hydrogen as fuel, however, continue to reduce the suitability and competitiveness of hydrogen fuel cells.

Recently, a novel energy storage system that incorporates electrically rechargeable liquid fuels was proposed and experimentally demonstrated [13]. Uniquely different from all the conventional energy storage systems, the innovative electrochemical system was developed such that the charge and discharge processes are independently achieved. The electrically rechargeable liquid fuels, known as e-fuels, which can be obtained from diverse range of electroactive materials, including but not limited to metal ions, were mentioned as excellent options for the energy storage medium. E-fuel cell is one of the two major components, the other is e-fuel charger, that constitute the e-fuel energy storage system. While the e-fuel charger solely charges the discharged e-fuel to be stored as energy, the e-fuel cell primarily generates electrical energy using the charged and stored e-fuel. This

latest system therefore characterizes a major step forward in the advancement of electrical energy storage and power generation systems. The e-fuel cell, in particular, has subsequently attracted increasing research attentions for power generation due its unique features and advantages. As a result of the flexibility of fuel that can be employed in the operation of the e-fuel cell, Shi et al. recently demonstrated the operation of a liquid e-fuel cell utilizing a liquid e-fuel containing vanadium ions at the anode paired with oxygen cathode [14]. Superior reactivity, long cycle life, instant recharging, wide operating temperature range, low environmental footprint, easy storage, and catalyst-free materials were mentioned as some of the merits of using this particular liquid e-fuel. The e-fuel cell was thus reported to achieve significant performances, higher than those of the conventional liquid fuel cells, which underscores its considerable potentials not only for stationary applications but also for fuel cell electric vehicles.

The physicochemical processes involved in the operation of this liquid e-fuel cell include the transport of various electroactive species (V^{2+}, V^{3+}, and H^{+}) and the neutral species (O_2 and water); ionic and electronic current flux through the porous media; ionic current flux which travels as protons through the proton exchange membrane; and the electrochemical reactions on the active surface of the porous media [15]. To better understand and garner more insights on the complex and highly coupled fluid flow, mass/charge transport processes, and electrochemical reactions which take place within the multi-layer porous structure of the cell, numerical studies are of paramount importance. In the open literature, it was found that Wandschneider et al. has developed a two-dimensional model for a vanadium oxygen fuel cell [16]. Their modeling geometry considered two membranes and an intermediate chamber between the anode and cathode half-cells. This is not a typical

fuel cell structure and may not be considered suitable to describe the transport behaviors and the simulation of the cell performance under real conditions and applications. Chen et al. also developed a one-dimensional model for a vanadium/oxygen redox fuel cell [17], which was achieved by simplifying the complexity of some phenomena that occur in the fuel cell system. Hence, the multi-dimensional effect of fluid flow and mass transport particularly at high current densities were not obtainable from the model.

In this work, we present a two-dimensional model to describe the transport behaviors and predict the performance of a liquid e-fuel cell using the typical structure of a fuel cell. The model involves fluid flow and mass/charge transport coupled with electrochemical reactions. To validate the mathematical model, the simulation results are compared with the experimental data and the comparison shows a good agreement. The vanadium-ion concentration distributions in the channels and the porous anode at some designated current densities are presented to further provide substantial information, such as local concentrations, useful for gaining in-depth insight into the operation of the e-fuel cell and simulation of its performance. The impacts of varying the operation variables, structural design parameters, and electrochemical parameters on the cell performance are further examined via numerical simulation.

2. Model Formulation

2.1 Physicochemical processes

The structure of a liquid e-fuel cell as shown in **Fig. 1** basically consists of a proton exchange membrane sandwiched between an anode and a cathode. The anode is a porous and catalytic layer, while the cathode consists of a diffusion layer and a catalyst layer. During the operation of the liquid e-fuel cell, the liquid e-fuel containing vanadium ions

and the pure oxygen are directly fed into the anode and the cathode flow channels of the cell, respectively. The e-fuel is thus transported to the matrix surface of the anode where the anodic reaction takes place. The anode reaction is given as follows [18]:

$$V^{2+} \rightarrow V^{3+} + e^{-} \qquad E_a^0 = -0.255\ V \qquad (1)$$

The consumption of V^{2+} at the anode side during the oxidation reaction results in concentration gradients of the electroactive species as the bulk liquid e-fuel flows from the channels to the surface of the porous anode. During this anodic reaction, electrons and protons are also released and transported to the cathode side through an external electrical circuit and the membrane, respectively.

At the cathode side of the cell, pure oxygen is supplied through the flow channels and directly flows through the cathode diffusion layer to the cathode catalyst layer. At the cathode catalyst layer, the oxygen reacts with the electrons and protons, arriving from the anode, for oxygen reduction reaction to produce water as follows [18]:

$$O_2 + 4e^{-} + 4H^{+} \rightarrow 2H_2O \qquad E_c^0 = +1.23\ V \qquad (2)$$

The resulting overall electrochemical reaction occurring in the liquid e-fuel cell is [18]:

$$4V^{2+} + O_2 + 4H^{+} \rightarrow 4V^{3+} + 2H_2O \qquad E^0 = 1.485\ V \qquad (3)$$

Where E_a^0, E_c^0, and E^0 represents the standard reduction potential of the anode, cathode, and the entire cell, respectively.

2.2 Model simplifications and assumptions

As described above, the operation of a liquid e-fuel cell clearly involves complex and multi-component transport processes coupled with electrochemical reactions. To simplify

the computational modeling of the physicochemical processes that take place in the liquid e-fuel cell, the following assumptions are taken into consideration:

1. Isotropic and homogeneous properties are assumed for the porous anode, membrane, cathode catalyst layer, and cathode diffusion layer.

2. Dilute-solution approximation describes the species transport at the anode, hence interactions among the ions in the e-fuel solution are neglected.

3. The e-fuel cell operations are assumed to be at isothermal and steady-state conditions.

4. The liquid e-fuel flow at the anode is taken as incompressible.

5. Liquid e-fuel, oxygen, and water crossover via the membrane are not considered.

6. Side reactions are also ignored.

2.3 Computational domains

Based on the very limited modeling studies on the liquid e-fuel cell, many parameters which influence its performance and optimization are evidently yet to be numerically investigated. Therefore, applying a complex geometric dimensionality, such as 3D for the whole study, at this stage may not be suitable due to the significant computational time and huge computing capacity facility required. Nonetheless, a 3D computational domain, shown in **Fig. 1a**, was employed to simulate the fluid flow process in the serpentine flow channel (2 cm x 2 cm) and the porous anode of the liquid e-fuel cell to obtain the pressure distribution of the fluid particularly in the flow channels. Thereafter, a 2D model was applied to perform the simulations of other phenomena and parameters while probing their effects on the overall performance of the liquid e-fuel cell. **Fig. 1b** shows the schematic of a liquid e-fuel cell and the 2D computational domain employed in this study.

2.4 Governing equations

2.4.1 Anode compartment

2.4.1.1 Fluid flow

In this model, the liquid e-fuel flowing through the single serpentine flow channel to the porous anode is described using the free and porous media flow which couples the free flow of the liquid e-fuel in the channels described by Navier–Stokes equation and the flow in the porous anode governed by Brinkman equation as follows [19]:

$$\rho(\vec{v}\cdot\nabla)\vec{v} = \nabla\cdot[-PI + \mu(\nabla\vec{v} + (\nabla\vec{v})^T)] \quad (4)$$

$$\frac{1}{\varepsilon^2}\rho(\vec{v}\cdot\nabla)\vec{v} = \nabla\cdot\left[-PI + \frac{\mu}{\varepsilon}(\nabla\vec{v} + (\nabla\vec{v})^T)\right] - \frac{2\mu}{3\varepsilon}\nabla(\nabla\cdot\vec{v})I - \frac{\mu}{k}\vec{v} \quad (5)$$

Where ρ is the liquid density, $\vec{v}$ is the liquid velocity, P is the liquid pressure, μ is the liquid viscosity, ε is the porosity of the anode, and the permeability, k, of the porous anode is described by Kozeny-Carman equation:

$$k = \frac{d^2\varepsilon^3}{180(1-\varepsilon)^2} \quad (6)$$

Where d is the fibre diameter of the porous anode.

It is worth to mention that no specific boundary condition was formulated at the interface between the flow channels and the porous anode as a result of mass and momentum continuity applied at this interface:

$$\rho\,\nabla\cdot\vec{v} = 0 \quad (7)$$

2.4.1.2 Mass/charge transport

The mass/charge transport taking place at the porous anode of the liquid e-fuel cell majorly involves the transport of the various electroactive species (i = V^{2+}, V^{3+}, and H^+) in the e-fuel solution, the ionic, and electronic current through the porous anode. The transport of

each electroactive specie, i, in the e-fuel solution is described by Nernst-Planck equation, where transport resulting from the interactions among the ions is ignored, such that the molar flux, $\vec{N}_i$, of each electroactive specie in the porous anode is given as [20]:

$$\vec{N}_i = -D_i^{eff}\nabla c_i - z_i c_i u_i F \nabla \emptyset_{a,l} + \vec{v} c_i \quad (8)$$

Where D_i^{eff} is the effective diffusion coefficient of the porous electrode, c_i is the concentration of species, z_i is the valence of species, u_i is ionic mobility, F is Faraday's constant, $\emptyset_{a,l}$ is ionic potential of liquid e-fuel, and $\vec{v}$ is the liquid e-fuel velocity.

The effective diffusion coefficient, D_i^{eff}, of each electroactive specie according to Bruggemann correction is expressed as:

$$D_i^{eff} = \varepsilon^{1.5} D_i \quad (9)$$

Where D_i is the diffusion coefficient of species and ε is the anode porosity.

The effective mobility, u_i, of each electroactive specie according to Nernst-Einstein equation in relations to the effective diffusion coefficient is given as:

$$u_i = \frac{D_i^{eff}}{RT} \quad (10)$$

Where R is the universal gas constant and T is operating temperature of the cell.

The conservation of mass for each electroactive specie in the porous anode at steady-state is given as [21]:

$$\nabla \cdot \vec{N}_i = S_i \quad (11)$$

Where the electrochemical reaction source term, S_i, for the electroactive species is given as:

$$S_i = \frac{v_i}{nF} a_a j_a \quad (12)$$

Where n is the number of electrons transferred from the anode, a_a is the active surface area of the anode, v_i is the stoichiometric coefficient of each electroactive specie participating in the electrochemical reaction at the porous anode where v_i is 1 and -1 for V^{2+} and V^{3+}, respectively (Equation 1) and j_a is the local current density at the porous anode.

The e-fuel solution, a mixture of vanadium ions and sulfuric acid, fed into the anode compartment of the e-fuel cell is considered to be electrically neutral such that the concentration of SO_4^{2-} from the dissociation of the sulfuric acid can be described by electroneutrality condition as follows [20]:

$$\sum_i z_i c_i = 0 \tag{13}$$

The porous anode is subjected to both ionic and electronic conductions for the purpose of charge transfer between the anode and the e-fuel solution. Hence the charge that leaves the e-fuel solution is expected to be balanced by the charge that enters the porous anode according to charge conservation expressed as [22, 23]:

$$\nabla \cdot \vec{i}_{a,l} = -\nabla \cdot \vec{i}_{a,s} = a_a j_a \tag{14}$$

Where the total ionic current, $\nabla \cdot \vec{i}_{a,l}$, due to the transfer of ions, i, in the e-fuel solution is expressed as:

$$\vec{i}_{a,l} = F \sum_i z_i \vec{N}_i \tag{15}$$

The electronic current, $\nabla \cdot \vec{i}_{a,s}$, in the porous anode described by ohm's law is expressed as:

$$\vec{i}_{a,s} = -\sigma_{a,s}^{eff} \nabla \emptyset_{a,s} \tag{16}$$

Where $\emptyset_{a,s}$ is the ionic potential of the anode and the effective electrical conductivity, $\sigma_{a,s}^{eff}$, of the anode is calculated according to Bruggemann correction expressed as:

$$\sigma_{a,s}^{eff} = (1-\varepsilon)^{1.5}\sigma_{a,s} \quad (17)$$

Where $\sigma_{a,s}$ is the electrical conductivity of the anode.

2.4.2 Membrane

The proton exchange membrane is assumed to be permeable to only protons in this study. Generally, membrane allows ionic but not electronic conduction, hence only ionic current transport exists in the membrane. The ionic current vector in the membrane, $\vec{\imath}_m$, is always in the direction of the proton flux, according to Faraday's law. However, current source is not produced in the membrane since charge consumption or generation via electrochemical reaction are not taking place in the membrane. The current conservation in the membrane is therefore expressed as [24]:

$$\nabla \cdot \vec{\imath}_m = 0 \quad (18)$$

Due to the absence of fluid flow and the fact that electroactive species crossover through the membrane is not considered in this model, the transport of protons through the membrane resulting from migration, majorly driven by potential gradient, is represented by ohm's law as follows [25]:

$$\vec{\imath}_m = -\sigma_m \nabla \emptyset_m \quad (19)$$

The flux of proton, $\vec{N}_{H^+}$, through the membrane is therefore expressed as [22]:

$$\vec{N}_{H^+} = \frac{\vec{\imath}_m}{F} = -\frac{\sigma_m}{F}\nabla \emptyset_m \quad (20)$$

Where σ_m and $\emptyset_m$ represent the ionic conductivity and ionic potential of the proton exchange membrane, respectively.

2.4.3 Cathode compartment

A diffusion layer and a catalyst layer are considered as the porous media at the cathode compartment of the e-fuel cell. Pure oxygen is delivered into the cell at the cathode side through the flow channels to the diffusion layer and to the surface of the catalyst layer where the oxygen reduction reaction takes place. Water is usually the major product of the electrochemical reaction at the cathode. The produced water, in addition to the water transferred from the anode, therefore flows via the diffusion layer, and exit through the outlet of the cathode flow channel. However, a simplified model of the cathode is used in this study where pure oxygen is assumed to be uniformly distributed at the cathode. In addition, the transport processes of water and oxygen at the cathode are not considered in this study. Nonetheless, the cathode catalyst layer is still subjected to both ionic and electronic conductions. The charge conservation at the cathode is therefore expressed as [26]:

$$\nabla \cdot \vec{\imath}_{c,l} = -\nabla \cdot \vec{\imath}_{c,s} = a_{ccl} j_c \tag{21}$$

Where a_{ccl} is the active surface area of the cathode catalyst layer, j_c is the local current density at the cathode, and the ionic current, $\nabla . \vec{\imath}_{c,l}$, at the cathode catalyst layer is expressed as:

$$\vec{\imath}_{c,l} = -\sigma_{c,l} \nabla \emptyset_{c,l} \tag{22}$$

The electronic current, $\nabla \cdot \vec{\imath}_{c,s}$, at the cathode catalyst layer described by ohm's law is expressed as:

$$\vec{\imath}_{c,s} = -\sigma_{c,s} \nabla \emptyset_{c,s} \tag{23}$$

$\emptyset_{c,l}$ and $\emptyset_{c,s}$ is the ionic potential and electronic potential at the cathode, respectively.

2.5 Electrochemical kinetics

2.5.1 Anode

The electrochemical reaction that occurs at the interface between the porous anode and the e-fuel solution is connected with local current density, j_a, and activation overpotential, η_a, of the anode. This interfacial reaction kinetic is governed and mathematically expressed by the Butler-Volmer equation given as [19]:

$$j_a = Fk_a\left(c_{V^{2+}}^{s}\right)^{\alpha_{1,a}}\left(c_{V^{3+}}^{s}\right)^{\alpha_{1,c}}\left[exp\left(\frac{\alpha_{1,a}F\eta_a}{RT}\right) - exp\left(-\frac{\alpha_{1,c}F\eta_a}{RT}\right)\right] \quad (24)$$

The exchange current density, $i_{0,a}$, for the reaction at the porous anode is given as:

$$i_{0,a} = Fk_a\left(c_{V^{2+}}^{s}\right)^{\alpha_{1,a}}\left(c_{V^{3+}}^{s}\right)^{\alpha_{1,c}} \quad (25)$$

Where k_a is the rate constant of the anodic reaction, s is surface, and $\alpha_{1,a}$ and $\alpha_{1,c}$ is the anodic and cathodic charge transfer coefficient at the anode, respectively.

The activation overpotential, η_a, for the reaction at the porous anode is described as:

$$\eta_a = \emptyset_{a,s} - \emptyset_{a,l} - E_a^{eq} \quad (26)$$

where the porous anode potential, E_a, is given as:

$$E_a = \emptyset_{a,s} - \emptyset_{a,l} \quad (27)$$

$\emptyset_{a,s}$ is the electric potential and $\emptyset_{a,l}$ is the electrolyte (liquid e-fuel) potential.

The equilibrium potential, E_a^{eq}, for the electrochemical reaction at the porous anode, equation (1), is determined using Nernst equation given as follows [20]:

$$E_a^{eq} = E_a^0 + \frac{RT}{F}\ln\left(\frac{c_{V^{3+}}}{c_{V^{2+}}}\right) \quad (28)$$

Where E_a^0 is the standard potential for the anodic reaction, R is the molar gas constant, T is the operating temperature of the cell, F is Faraday's constant, and c is the concentration of the corresponding specie.

2.5.2 Cathode

At the cathode catalyst layer, a simplified Butler-Volmer equation is used to describe the local current density, j_c, as follows [27]:

$$j_c = i_{0,c}\left[exp\left(-\frac{\alpha_{2,c}F\eta_c}{RT}\right)\right] \quad (29)$$

The activation overpotential, η_c, at the cathode is described as:

$$\eta_c = \emptyset_{c,s} - \emptyset_{c,l} - E_c^{eq} \quad (30)$$

where the cathode potential, E_c, is given as:

$$E_c = \emptyset_{c,s} - \emptyset_{c,l} \quad (31)$$

Where $i_{0,c}$ is the cathodic exchange current density, $\alpha_{2,c}$ is the cathodic charge transfer coefficient at the cathode, and E_c^{eq} is the equilibrium potential at the cathode.

2.6 Boundary conditions

2.6.1 Boundary conditions for momentum balance

A fully developed flow boundary condition, at a specified flow rate, is applied at the inlet of the flow channel such that the velocity profile as well as the momentum does not change in the fluid flow direction. Pressure boundary condition is applied at the outlet of the 3D computational domain for the anode flow channel with a zero-pressure value as follows:

$$\begin{cases} \vec{v} = v_{in} = {Q_a}/{A} \\ P = P_{out} = 0 \end{cases} \quad (32)$$

Where Q_a is the volumetric flow rate of the e-fuel, and A is the cross-sectional area of the flow channel.

In addition, no-slip boundary and no specie flux conditions are applied to the walls of both the flow channels and the porous anode such that:

$$\vec{v}_{wall} = 0 \quad (33)$$

In the 2D computational domain, pressure boundary condition is applied at each flow channel. The value of each pressure used in the 2D model is the pressure obtained at the midpoint of each channel on yz-planes as shown in **Fig. 1a** from the 3D simulation of the fluid flow. No-slip wall boundary condition is also applied to the walls of both the flow channels and porous anode in the 2D model.

2.6.2 Boundary conditions for mass/charge balance

At the anode, ten sections of the 3D flow channels were selected to represent the flow channel in the 2D model. Hence, the concentration of the e-fuel applied at each section of the channel in the 2D model is calculated based on the assumption that the concentration drop of the e-fuel in the 3D flow channel is linear. Since the 3D flow channel is a single domain, the concentration of the e-fuel at the outlet of the 3D flow channel is determined as follows:

$$c_{v^{2+}}^{f} = c_{v^{2+}}^{0} - \frac{iA_{cell}}{FQ_a} \tag{34}$$

Where $c_{v^{2+}}^{f}$ is the e-fuel concentration at outlet, $c_{v^{2+}}^{0}$ is the initial e-fuel concentration at inlet, i is the applied current density, A_{cell} is the area of the cell, F is Faraday's constant, and Q_a is the e-fuel flow rate.

Hence, the overall e-fuel concentration drop, $\Delta c_{v^{2+}}$, in the 3D flow channel is:

$$\Delta c_{v^{2+}} = c_{v^{2+}}^{0} - c_{v^{2+}}^{f} = \frac{iA_{cell}}{FQ_a} \tag{35}$$

The e-fuel concentration drops at each selected sections of the channel used in the 2D is derived as follows:

$$\Delta c_{v^{2+}}^{l} = \Delta c_{v^{2+}} \times \frac{l}{L} \tag{36}$$

Where l is the distance of each selected section from the inlet of the 3D flow channel and L is the entire length of the 3D flow channel.

Thus, the e-fuel concentration at each section is:

$$c_{v^{2+}}^{l} = c_{v^{2+}}^{0} - \Delta c_{v^{2+}}^{l} \tag{37}$$

At the current collector and porous anode interface, the electric potential at the boundary is taken as zero:

$$\emptyset_{a,s} = 0 \tag{38}$$

The boundary condition of the flux at the interface between the porous anode and the membrane is given as:

$$\begin{cases} \vec{N}_i = 0 \ (i \neq H^+) \\ \vec{N}_{H^+} = -\frac{\vec{\imath}_{a,l}}{F} \end{cases} \tag{39}$$

At the porous anode and membrane interface, the ionic current density is regarded to be continuous:

$$\nabla \cdot \vec{\imath}_{a,l} = \nabla \cdot \vec{\imath}_m \tag{40}$$

The ionic potential at the porous anode and membrane interface, is taken to be continuous such that Donnan potential is not considered at this interface as follows:

$$\emptyset_{a,l} = \emptyset_m \tag{41}$$

Similarly, at the membrane and cathode catalyst layer interface, the electrolyte potential is expressed as:

$$\emptyset_{c,l} = \emptyset_m \tag{42}$$

To maintain the charge conservation, the electronic current density from the cathode is equal to the applied current density as follows:

$$\vec{\imath}_{c,s} = i \tag{43}$$

2.7 Cell voltage

The cell voltage is the electric potential difference between the cathode and the anode. It is therefore derived at the external boundary of the cathode, that is, at the interface between the cathode diffusion layer and the current collector given as:

$$V_{cell} = \emptyset_{c,s} - \emptyset_{a,s} \quad (44)$$

As mentioned earlier, the electric potential, $\emptyset_{a,s}$, at the current collector and porous anode interface is zero.

Therefore, $V_{cell} = \emptyset_{c,s}$ (45)

All the equations above are numerically solved using COMSOL Multiphysics. **Tables 1-4** show the cell geometry properties and porous media parameters, e-fuel solution parameters and operating conditions, physicochemical parameters, and mass/charge transport parameters.

3. Results and discussion

3.1 Model validation

In this section, the cell voltages at three different concentrations of e-fuel are examined and compared with experimental data to validate the fidelity of the model. The experimental data were obtained from a study where the liquid e-fuel cell employing various concentrations of e-fuel solution was operated at 23 ℃ [14]. The simulated results, in comparison with the experimental data, showing the polarization curves of different initial concentrations of the e-fuel solution at 0.1 M, 0.3 M, and 0.5 M V^{2+}, each mixed with 3.0 M H_2SO_4, are displayed in **Fig. 2**. For the purpose of this validation, the operating condition of the model is in accordance with that of the experiment. For instance, the flow rate of the e-fuel is kept at 20.0 mL min^{-1}. It is shown that the simulated cell performances

all show a good agreement with the experimental data capturing the activation, ohmic, and transport loss regions. The simulation results clearly show that the cell performance significantly improves when the vanadium-ion concentration in the e-fuel solution increases from 0.1 M to 0.5 M. This is because local concentrations of vanadium-ion at the anode of the cell increase with its initial concentration as a result of the enhanced mass transport of the vanadium-ion. Consequently, the electrochemical kinetics of the reaction at the anode is further improved and the concentration loss is considerably minimized due to the higher concentration of V^{2+} employed. The simulated cell voltage mostly shows a linear drop with increasing current density before falling off to the limiting current density of approximately 160, 423, and 650 mA cm^{-2} for e-fuel concentrations containing 0.1 M, 0.3 M, and 0.5 M V^{2+}, respectively, apparently due to mass transport loss. The mass transport loss is attributed to the concentration gradient between the bulk e-fuel solution and the surface of the porous anode, particularly at high current densities [28]. However, a further increase of the initial vanadium-ion concentration, beyond 0.5 M, could deteriorate the cell performance due to a corresponding increase in charge transfer resistance [14]. A relatively high concentration of vanadium-ion at the anode is therefore suggested to be of beneficial effects on the cell performance.

As the performance of the cell is significantly influenced by the e-fuel concentration, the presentation of the vanadium-ion concentration distribution at the anode is of paramount importance towards understanding and investigating the operations of the e-fuel cell. To this end, the vanadium-ion concentration distributions in the flow channel and porous anode at designated current densities when the cell is fed with an e-fuel solution containing the three different concentrations of V^{2+} are displayed. The trend and changes in vanadium-

ion concentration distributions at various current densities are presented to justify the concentration loss and the limiting current densities. While **Figs. 3a, 4a, and 5a** show the polarization curves, **Figs. 3b, 4b, and 5b** show the concentration distribution of the vanadium-ion when the cell is fed with an e-fuel solution containing 0.1 M, 0.3 M, and 0.5 M V^{2+}, respectively. It can be seen that, at the three initial concentrations considered, the concentration distribution of vanadium-ion decreases in the flow channels and the porous anodes with increasing current density. This is because the vanadium-ion is rapidly consumed at higher current density. This therefore reveals and explains the reason the vanadium-ion is almost completely diminished when the e-fuel cell operates at current densities close to the limiting current density. Beyond the limiting current density, the concentration of the e-fuel is already extremely low or completely consumed at the anode compartment thereby leading to low reaction rate and large mass transport losses. In the subsequent sections, the results of the numerical simulations showing the influence of various operation variables, structural design parameters, and electrochemical parameters on the cell performance are presented.

3.2 Effect of operating parameters

3.2.1 Effect of the sulfuric acid concentration

The anode side of this liquid e-fuel cell houses the fuel as well as serves as the proton source due to the type of e-fuel solution (containing 0.5 M V^{2+} and H_2SO_4) employed in the cell operation. The sulfuric acid (H_2SO_4) functions as the supporting electrolyte, which can dissociate into H^+ and SO_4^{2-} at the anode compartment [23, 29]. As mentioned earlier, the operation of the e-fuel cell involves the transport of protons (H^+) from the anode through the membrane which subsequently participate in the electrochemical reactions

occurring at the cathode side as given in Equation (2). The composition of the e-fuel solution would therefore certainly influence the concentration of H^+ and thus the cell performance. Here, the effect of various concentration of sulfuric acid on the cell performance is examined and presented in **Fig. 6a**. It is seen from **Fig. 6a** that the cell performance improves with increasing sulfuric acid concentration, which are more pronounced at higher current densities. For instance, at 600 mA cm^{-2}, the cell voltage increases from 0.461 V to 0.538 V when the sulfuric acid concentration is increased from 1.0 M to 4.0 M. In addition, the maximum current density also increases with the sulfuric acid concentration. The performance improvement can be attributed to the fact that higher sulfuric acid concentration leads to higher concentration distribution of H^+ at the anode and its transport near the membrane as evidenced in **Fig. S1**. This therefore facilitates the transport of protons to the membrane thereby reducing ohmic loss. The increase in cell voltage at high current densities indicates that a relatively high sulfuric acid concentration can contribute to the improvement of the cell performance. However, it is also worth to mention that, since the cell performance shows no obvious difference at the low to middle current density range with the increase of sulfuric acid concentration, especially from 3.0 M to 4.0 M, it may not be suitable for the cell to use the e-fuel with a sulfuric acid concentration higher than 3.0 M. This is because the viscosity of the e-fuel solution increases with increasing the sulfuric acid concentration and could lead to an undesirable increase in charge transfer resistance [30], such that the use of a higher sulfuric acid concentration would not only reduce the energy density of the system, but also create a more corrosive environment inside the cell thereby deteriorating the chemical stability of cell components.

3.2.1 Effect of the e-fuel flow rate

In addition to the e-fuel and the sulfuric acid concentration, the e-fuel flow rate is another significant operating condition which notably influences the electrochemical performance of the e-fuel cell. The e-fuel cell is energized through the flowing of the liquid e-fuel, hence the mass transport process as well as the performance of the cell would largely be influenced by the e-fuel flow rate. In other words, the flow rate governs the magnitude of the e-fuel entering the cell and also determines the distribution of the e-fuel solution and electroactive species particularly at the anode. In this section, the effect of different e-fuel flow rates ranging from 5.0 to 20.0 mL min^{-1}, on the cell performance are numerically examined. Considering an e-fuel solution containing 0.5 M V^{2+} and 3.0 M H_2SO_4, the cell performance obviously improves with increase in the e-fuel flow rate as shown in **Fig. 6b**. This is primarily due to the fact that higher e-fuel flow rate facilitates rapid and sufficient distribution of reactants at the anode as shown in **Fig. S2**. Mass transport limitation is also evidently reduced when the cell performance is further examined at a higher flow rate of 30.0 mL min^{-1} as shown in **Fig. S3**. It can also be seen that the limiting current density increases with the e-fuel flow rate resulting from higher flux of the e-fuel solution from the flow channel to the surface of the porous anode for rapid electrochemical reaction. In addition, higher e-fuel flow rates also favor rapid transport of hydrogen ions to the membrane as more hydrogen ions are seen near the membrane in comparison to when the cell is operated at low e-fuel flow rate as presented in **Fig. S4**. However, operating the cell at higher flow rates would involve additional pump power consumption which in turn deteriorates the efficiency of the e-fuel cell system [31]. This therefore highlights the need to further investigate the optimal flow rate suitable for the operation of this e-fuel cell.

3.3 Effect of structural design parameters

3.3.1 Effect of anode porosity

During the operation of the liquid e-fuel cell, the electroactive species in the e-fuel solution are transferred through the pores of the anode to the active surface area of the anode for electrochemical reaction to take place. Thus, the porous structure and properties of the anode exert a considerable impact on the transport processes as well as the performance of the cell [32]. The effects of anode porosity, as one of the critical structural design parameters, on the e-fuel cell performance is numerically investigated in this section. **Fig. 7a** displays the polarization curves to demonstrate the effect of various anode porosities on the cell performance. It is found that when the anode porosity increases from 0.70 to 0.85, the cell performance significantly improves. This is primarily because higher anode porosity promotes higher permeability of the anode to fluid flow and further increases the supply and concentration distribution of vanadium-ion for the electrochemical reaction such that the depletion rate of the reactants at the anode is reduced, which is evidenced by **Fig. S5**. The mass transport process is therefore improved with increase in anode porosity. Consequently, concentration polarization resulting from mass transport loss, which could limit the current density of the cell, is significantly reduced. This is obvious at the highest anode porosity of 0.85 as no mass transport loss is observed. As a result, the overall overpotential at the anode decreases as the anode porosity increases to improve cell performance. In summary, an increase in anode porosity increases the fluid permeability and the effective diffusion coefficient of the anode which all contribute to an improvement in the overall cell performance.

3.3.2 Effect of anode thickness

The thickness of anode is another significant structural design parameter that influences transport pathway, which includes the transport of active species, ions, and electrons, at the anode, distribution of electroactive species, and thus the performance of the e-fuel cell [33]. For this reason, different anode thicknesses were employed, while the dimension of other components remain unchanged, to evaluate their influence on the cell performance. **Fig. 7b** presents the simulated polarization behavior of the e-fuel cell at different anode thicknesses (1, 2, and 3 mm). This figure shows that the cell performance increases with the anode thickness. When the anode thickness is increased from 1 to 3 mm, the cell voltage is seen to increase over the entire current density range and attain higher maximum current density. The observed improvement in the cell performance can be attributed to the fact that a thicker anode increases the total surface area of anode, which is not only essential for enhanced distribution of vanadium-ion at the anode as shown in **Fig. S6,** but also for rapid electrochemical reaction, thereby reducing activation overpotential. The anode overpotential therefore decreases with increase of anode thickness from 1mm to 3 mm to enhance the cell performance. However, it is also worth to mention that a large increase of the anode thickness could elongate the charge transfer pathway in the anode which in turn would increase charge transport resistance and ohmic loss at the anode. It can therefore be concluded that when a relatively thicker anode is applied, the operations and performance of the e-fuel cell improves, particularly at high current densities.

3.3.3 Effect of membrane thickness

Membrane is one of the key components in the structural design of a typical fuel cell primarily to separate the anode and cathode compartments thereby preventing the crossover

of electroactive species. Membrane in a fuel cell is also essential for providing pathways for ionic transport between the anode and the cathode. To prevent electrical short circuit within the cell is another significant function of the membrane [33-35]. Membrane properties such as thickness will heavily influence the transport of ions through the membrane and thus the overall cell performance. Therefore, the effect of membrane thickness on the performance of this liquid e-fuel cell is studied in this section and the results at varying membrane thicknesses are shown in **Fig. 7c**. The cell voltage is found to decrease with increase of membrane thickness at all the current density range considered. For instance, the cell voltage drops from 0.684 V to 0.469 V at current density of 500 mA cm^{-2} with respect to increase of membrane thickness from 100 μm to 400 μm. The degradation of cell performance is due to increase in the distance of ionic transport in thicker membrane, which thereby leads to a higher membrane ohmic resistance and further increase the membrane overpotential. It is worth to mention that, at a membrane thickness higher than 300 μm, due to the large membrane overpotential induced by the increase of membrane ohmic resistance, no concentration polarization is observed before the cell voltage drops to 0.4 V. Conversely, when using thinner membranes, for instance from 200 μm to 50 μm as shown in **Fig. 7c**, the cell is able to operate at over 650 mA cm^{-2} due to the reduced ohmic loss, which thereby induced the concentration loss at the end of the polarization curve. This therefore suggests that a thinner membrane, in comparison to thicker membranes, is required and preferable for better performance of the e-fuel cell. However, it is worth mentioning that the drawbacks of employing thinner membrane could be its vulnerability to high crossover of species [36]. Although the crossover phenomena

are not included this study due to the assumption that the membrane is only permeable to protons.

3.3.4 Effect of cathode catalyst layer thickness

The cathode catalyst layer is one of the porous media, alongside the cathode diffusion layer, at the cathode compartment of the e-fuel cell. The cathode catalyst layer serves as the active site for the electrochemical reactions taking place at the cathode. The properties of the cathode catalyst layer such as thickness will thus influence the transport process of ions and electrons, active surface area, and also affect the general performance of the cell. **Fig. 7d** displays the polarization curves of the cell when the cathode catalyst layer thickness is varied. An upgrade in the cell voltage is clearly seen throughout the whole current density range as thicker cathode catalyst layer is applied. At a high current density of 600 mA cm^{-2}, the cell voltage attained when varying cathode catalyst layer thicknesses (1 μm, 10 μm, 20 μm, and 100 μm) are used for the cell simulation are 0.463 V, 0.528 V, 0.546 V, and 0.575 V, respectively. This apparent performance improvement can be attributed to the fact that thicker cathode catalyst layer provides more surface area for the electrochemical reactions at the cathode which therefore reduces activation loss. An increase in the thickness of the cathode catalyst layer significantly reduces the cathode overpotential and therefore increases the cell voltage. However, it should also be mentioned that employing a thicker cathode catalyst layer could elongate the transport process, particularly the diffusion of species at the cathode. In summary, a relatively thick cathode catalyst layer significantly contributes to the improvement of the e-fuel cell performance.

3.4 Effect of electrochemical parameters

3.4.1 Effect of anodic and cathodic exchange current density

The performance of the e-fuel cell is largely dependent upon the electrochemical parameters such as the electrocatalytic activity of the cathode catalyst layer and the electrochemical reaction kinetics at the anode and the cathode. For instance, the exchange current density is generally employed to demonstrate the electrochemical activities occurring at the anode and cathode. The influence of various anodic and cathodic exchange current densities on the cell performance are thus examined. It can be seen from **Fig 8a** that the cell voltage improves with increase in anodic exchange current density. For example, the cell voltage rises from 0.528 V to 0.663 V at current density of 600 mA cm^{-2} following the increase of the anodic exchange current density from 6.75 A m^{-2} to 164 A m^{-2}. This can be explained with the significant reduction of the anode overpotential as the anodic exchange current density increases. Similar trend is observed at the cathode. At current density of 600 mA cm^{-2}, the cell voltage is found increase up to 0.667 V from 0.459 V when the cathodic exchange current density is increased from 1.0 x 10^{-8} A m^{-2} to 1.0 x 10^{-5} A m^{-2} as depicted in **Fig. 8b.** This is also due to the corresponding reduction in the overpotentials at the cathode. At both anode and cathode, the highest exchange current density yields the highest cell voltage and superior cell performance for the entire current density considered in this study. In comparison, the cathodic exchange current density is much lower than the anodic due to the slow reaction kinetics of oxygen reduction reaction at the cathode. This therefore underscores the necessity of employing porous anodes of high electrochemical activity and an excellent active catalyst material at the cathode to enhance the exchange current densities of their electrochemical reactions.

4. Conclusion

In this work, a two-dimensional model describing the transport behaviors and predicting the performance of a liquid e-fuel cell is presented. The model incorporates fluid flow and mass/charge transport coupled with electrochemical reactions and it is the first model framework to describe the underlying theoretical and working principle of this liquid e-fuel cell using a typical fuel cell structure. The comparison of the results from the model simulation shows a good agreement with experimental data obtained from open literature. The concentration distributions of vanadium-ion, which cannot be obtained by experimental approach, show that a relatively high initial concentration results to high local concentration distribution of the e-fuel at the anode and that the e-fuel is rapidly consumed with increasing current density. It is also found that the cell voltage increases with the e-fuel concentration resulting from improved reaction kinetics of the e-fuel and increase in the mass transport process, thereby reducing the concentration polarization. Regarding the effects of the other operating conditions investigated, the cell performance improves with increase of the sulfuric acid concentration as well as the e-fuel flow rate. As for the structural design parameters, an increase in anode porosity, anode thickness, and cathode catalyst layer thickness all boosts the cell performance, whereas the cell voltage is found to decrease with increasing membrane thickness. Furthermore, the exchange current density at the anode and the cathode was shown to markedly influence the performance of the e-fuel cell following the significant reduction in their overpotential to improve cell voltage as the exchange current densities increase. This study therefore provides the essential basis useful for the extension and improvement of the e-fuel cell model towards optimizing the design and maximizing performance of the cell. Besides the transport of

protons through the membrane, the operation of the cell in practical scenario involves inevitable transport of the e-fuel and oxygen across the membrane. In addition, there is tendency for water to be transported towards the cathode from the anode, which also contributes to water accumulation at the cathode. These crossover phenomena often lead to side reactions, ohmic loss, and performance loss of the cell. These therefore highlight the incorporation and investigation of crossover phenomena including e-fuel, oxygen, and water transfer across the membrane as a potential direction for future work on this model.

Acknowledgement

The work described in this paper was fully supported by a grant from the Research Grant Council of the Hong Kong Special Administrative Region, China (Project No. T23-601/17-R).

References

[1] D. Larcher and J.-M. Tarascon, "Towards greener and more sustainable batteries for electrical energy storage," *J Nature chemistry,* vol. 7, no. 1, pp. 19-29, 2015.
[2] S. Chu, Y. Cui, and N. Liu, "The path towards sustainable energy," *Nature materials,* vol. 16, no. 1, pp. 16-22, 2017.
[3] R. C. Armstrong *et al.*, "The frontiers of energy," *Nature Energy,* vol. 1, no. 1, pp. 1-8, 2016.
[4] Z. Yang *et al.*, "Electrochemical energy storage for green grid," *Chemical reviews,* vol. 111, no. 5, pp. 3577-3613, 2011.
[5] J. W. Ager and A. A. Lapkin, "Chemical storage of renewable energy," *Science,* vol. 360, no. 6390, pp. 707-708, 2018.
[6] O. C. Esan, X. Shi, Z. Pan, X. Huo, L. An, and T. Zhao, "Modeling and Simulation of Flow Batteries," *Advanced Energy Materials,* vol. 10, no. 31, p. 2000758, 2020.
[7] L. Carrette, K. Friedrich, and U. Stimming, "Fuel cells-fundamentals and applications," *Fuel cells,* vol. 1, 2001.
[8] H. Chen, T. N. Cong, W. Yang, C. Tan, Y. Li, and Y. Ding, "Progress in electrical energy storage system: A critical review," *Progress in natural science,* vol. 19, no. 3, pp. 291-312, 2009.
[9] S. Changizian, P. Ahmadi, M. Raeesi, and N. Javani, "Performance optimization of hybrid hydrogen fuel cell-electric vehicles in real driving cycles," *International Journal of Hydrogen Energy,* 2020.

[10] S. T. Thompson *et al.*, "Direct hydrogen fuel cell electric vehicle cost analysis: System and high-volume manufacturing description, validation, and outlook," *Journal of Power Sources*, vol. 399, pp. 304-313, 2018.
[11] D.-Y. Lee, A. Elgowainy, A. Kotz, R. Vijayagopal, and J. Marcinkoski, "Life-cycle implications of hydrogen fuel cell electric vehicle technology for medium-and heavy-duty trucks," *Journal of Power Sources*, vol. 393, pp. 217-229, 2018.
[12] M. Granovskii, I. Dincer, and M. A. Rosen, "Economic and environmental comparison of conventional, hybrid, electric and hydrogen fuel cell vehicles," *Journal of Power Sources*, vol. 159, no. 2, pp. 1186-1193, 2006/09/22/ 2006, doi: https://doi.org/10.1016/j.jpowsour.2005.11.086.
[13] H. Jiang, L. Wei, X. Fan, J. Xu, W. Shyy, and T. Zhao, "A novel energy storage system incorporating electrically rechargeable liquid fuels as the storage medium," *J Science Bulletin*, vol. 64, no. 4, pp. 270-280, 2019.
[14] X. Shi, X. Huo, Y. Ma, Z. Pan, and L. An, "Energizing Fuel Cells with an Electrically Rechargeable Liquid Fuel," *Cell Reports Physical Science*, vol. 1, no. 7, p. 100102, 2020.
[15] X. Su, Z. Pan, L. An, and Y. Yu, "Mathematical modeling of direct formate fuel cells incorporating the effect of ion migration," *International Journal of Heat and Mass Transfer*, vol. 164, p. 120629, 2021.
[16] F. Wandschneider *et al.*, "A coupled-physics model for the vanadium oxygen fuel cell," *Journal of Power Sources*, vol. 259, pp. 125-137, 2014.
[17] C. L. Chen, H. K. Yeoh, and M. J. E. T. Chakrabarti, "One Dimensional Mathematical Modelling of the All-Vanadium and Vanadium/Oxygen Redox Flow Batteries," *ECS Transactions*, vol. 66, no. 10, p. 1, 2015.
[18] J. Noack, C. Cremers, D. Bayer, J. Tübke, and K. Pinkwart, "Development and characterization of a 280 cm2 vanadium/oxygen fuel cell," *Journal of Power Sources*, vol. 253, pp. 397-403, 2014.
[19] B. Zhang, Y. Lei, B. Bai, and T. Zhao, "A two-dimensional model for the design of flow fields in vanadium redox flow batteries," *International Journal of Heat and Mass Transfer*, vol. 135, pp. 460-469, 2019.
[20] A. Shah, M. Watt-Smith, and F. Walsh, "A dynamic performance model for redox-flow batteries involving soluble species," *Electrochimica Acta*, vol. 53, no. 27, pp. 8087-8100, 2008.
[21] M. Messaggi *et al.*, "Analysis of flow field design on vanadium redox flow battery performance: Development of 3D computational fluid dynamic model and experimental validation," *Applied energy*, vol. 228, pp. 1057-1070, 2018.
[22] X. Zhou, T. Zhao, L. An, Y. Zeng, and X. Yan, "A vanadium redox flow battery model incorporating the effect of ion concentrations on ion mobility," *Applied Energy*, vol. 158, pp. 157-166, 2015.
[23] K. Knehr, E. Agar, C. Dennison, A. Kalidindi, and E. Kumbur, "A transient vanadium flow battery model incorporating vanadium crossover and water transport through the membrane," *Journal of The Electrochemical Society*, vol. 159, no. 9, p. A1446, 2012.
[24] M. Vynnycky, "Analysis of a model for the operation of a vanadium redox battery," *Energy*, vol. 36, no. 4, pp. 2242-2256, 2011.

[25] S. Smith, I. Firdous, Q. Wang, S. Esmalla, and W. A. Daoud, "A two-dimensional model of the vanadium–cerium redox flow battery," *Electrochimica Acta,* vol. 328, p. 135019, 2019.
[26] Y. Wang, D. Sauer, S. Koehne, and A. Ersoez, "Dynamic modeling of high temperature PEM fuel cell start-up process," *International journal of hydrogen energy,* vol. 39, no. 33, pp. 19067-19078, 2014.
[27] D. G. Caglayan, B. Sezgin, Y. Devrim, and I. Eroglu, "Three-dimensional modeling of a high temperature polymer electrolyte membrane fuel cell at different operation temperatures," *international journal of hydrogen energy*, vol. 41, no. 23, pp. 10060-10070, 2016.
[28] A. Tang, J. Bao, and M. Skyllas-Kazacos, "Studies on pressure losses and flow rate optimization in vanadium redox flow battery," *Journal of power sources,* vol. 248, pp. 154-162, 2014.
[29] M. Vynnycky and M. Assunção, "On the significance of sulphuric acid dissociation in the modelling of vanadium redox flow batteries," *Journal of Engineering Mathematics,* vol. 123, no. 1, pp. 173-203, 2020.
[30] Y. Zhao, L. Liu, X. Qiu, and J. Xi, "Revealing sulfuric acid concentration impact on comprehensive performance of vanadium electrolytes and flow batteries," *Electrochimica Acta,* vol. 303, pp. 21-31, 2019.
[31] A. Khazaeli, A. Vatani, N. Tahouni, and M. H. Panjeshahi, "Numerical investigation and thermodynamic analysis of the effect of electrolyte flow rate on performance of all vanadium redox flow batteries," *Journal of Power Sources,* vol. 293, pp. 599-612, 2015.
[32] K. Oh, S. Won, and H. Ju, "Numerical study of the effects of carbon felt electrode compression in all-vanadium redox flow batteries," *J Electrochimica Acta,* vol. 181, pp. 13-23, 2015.
[33] X. Zhou, T. Zhao, L. An, Y. Zeng, and L. Wei, "Critical transport issues for improving the performance of aqueous redox flow batteries," *Journal of Power Sources,* vol. 339, pp. 1-12, 2017.
[34] X. Su, Z. Pan, and L. An, "Ion transport characteristics in membranes for direct formate fuel cells," *Frontiers in Chemistry*, vol. 8, p. 765, 2020.
[35] X. Shi *et al.*, "Polymer Electrolyte Membranes for Vanadium Redox Flow Batteries: Fundamentals and Applications," *Progress in Energy and Combustion Science*, vol. 85, p. 100926, 2021.
[36] S. Won, K. Oh, and H. Ju, "Numerical analysis of vanadium crossover effects in all-vanadium redox flow batteries," *Electrochimica Acta,* vol. 177, pp. 310-320, 2015.
[37] Y. Wang and S. C. Cho, "Analysis and three-dimensional modeling of vanadium flow batteries," *Journal of The Electrochemical Society*, vol. 161, no. 9, p. A1200, 2014.
[38] M. Li *et al.*, "Mesoscopic modeling and characterization of the porous electrodes for vanadium redox flow batteries," *Journal of Energy Storage,* vol. 32, p. 101782, 2020.
[39] W. Yang, Y. He, and Y. Li, "Performance modeling of a vanadium redox flow battery during discharging," *Electrochimica Acta*, vol. 155, pp. 279-287, 2015.

[40] M. Haghayegh, M. H. Eikani, and S. Rowshanzamir, "Modeling and simulation of a proton exchange membrane fuel cell using computational fluid dynamics," *International Journal of Hydrogen Energy*, vol. 42, no. 34, pp. 21944-21954, 2017.
[41] M. Ghasabehi, M. Ashrafi, and M. Shams, "Performance analysis of an innovative parallel flow field design of proton exchange membrane fuel cells using multiphysics simulation," *Fuel*, vol. 285, p. 119194, 2021.
[42] D. Cheddie and N. Munroe, "Parametric model of an intermediate temperature PEMFC," *Journal of Power Sources*, vol. 156, no. 2, pp. 414-423, 2006.
[43] P. Hong, L. Xu, J. Li, and M. Ouyang, "Modeling of membrane electrode assembly of PEM fuel cell to analyze voltage losses inside," *Energy*, vol. 139, pp. 277-288, 2017.
[44] S. Zhang, S. Beale, U. Reimer, M. Andersson, and W. Lehnert, "Polymer electrolyte fuel cell modeling-A comparison of two models with different levels of complexity," *International Journal of Hydrogen Energy*, vol. 45, no. 38, pp. 19761-19777, 2020.
[45] Q. Wang, Z. Qu, Z. Jiang, and W. Yang, "Numerical study on vanadium redox flow battery performance with non-uniformly compressed electrode and serpentine flow field," *Applied Energy*, vol. 220, pp. 106-116, 2018.

Figure captions

Fig. 1. (a) Schematic of the 3D computational domain for flow channels; (b) Schematic of a liquid e-fuel cell and the 2D computational domain.

Fig. 2. Comparison of the simulation results and experimental data [14].

Fig. 3. (a) Polarization curve when the cell is fed with an e-fuel solution containing 0.1 M V^{2+} in 3.0 M H_2SO_4. (b) Vanadium-ion concentration distributions at designated current densities – A. 20, B. 60, C. 100, D. 160, and E. 163 mA cm^{-2}.

Fig. 4. (a) Polarization curve when the cell is fed with an e-fuel solution containing 0.3 M V^{2+} in 3.0 M H_2SO_4. (b) Vanadium-ion concentration distributions at designated current densities - A. 100, B. 200, C. 300, D. 423, and E. 431 mA cm^{-2}.

Fig. 5. (a) Polarization curve when the cell is fed with an e-fuel solution containing 0.5 M V^{2+} in 3.0 M H_2SO_4. (b) Vanadium-ion concentration distributions at designated current densities - A. 100, B. 300, C. 500, D. 650, and E. 680 mA cm^{-2}.

Fig. 6. Effect of the (a) sulfuric acid concentration and (b) e-fuel flow rate on the cell performance.

Fig. 7. Effect of the (a) anode porosity, (b) anode thickness, (c) membrane thickness, and (d) cathode catalyst layer thickness on the cell performance.

Fig. 8. Effect of the (a) anodic and (b) cathodic exchange current densities on the cell performance.

Table captions:

Table 1. Cell geometry properties and porous media parameters.

Table 2. E-fuel solution parameters and operating conditions.

Table 3. Physicochemical parameters.

Table 4. Mass/charge transport parameters at the anode.

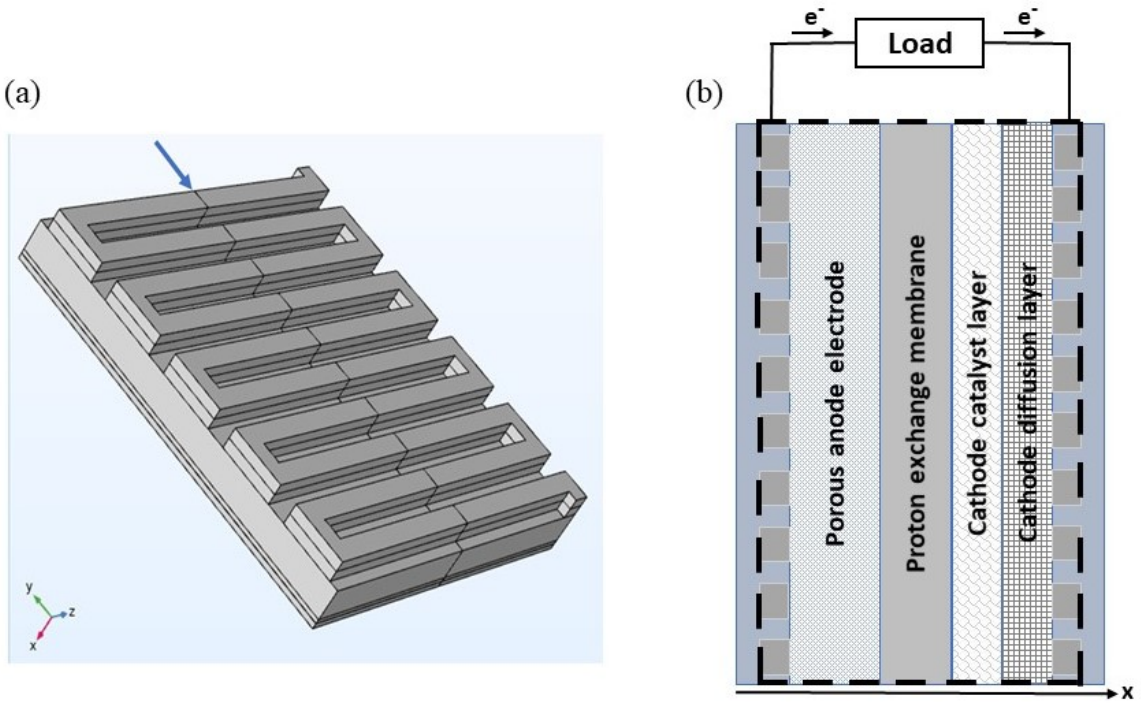

Fig. 1. (a) Schematic of the 3D computational domain for flow channels; (b) Schematic of a liquid e-fuel cell and the 2D computational domain.

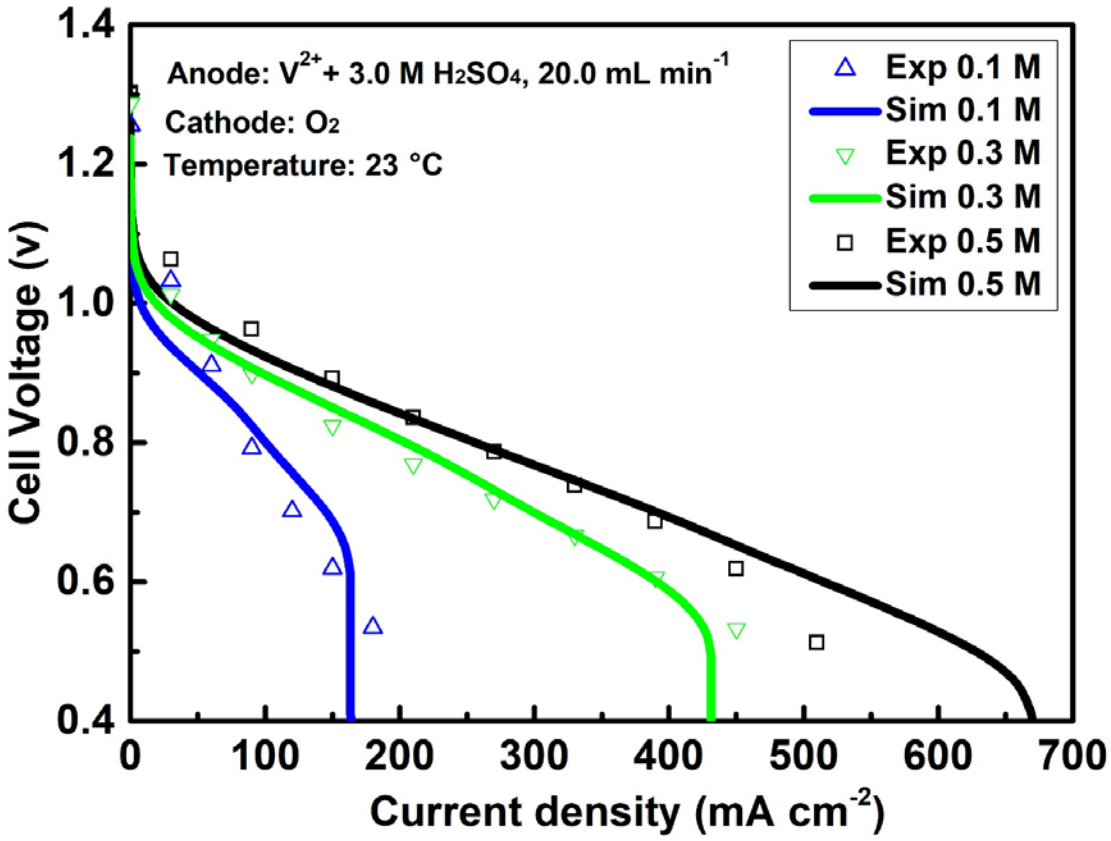

Fig. 2. Comparison of the simulation results and experimental data [14].

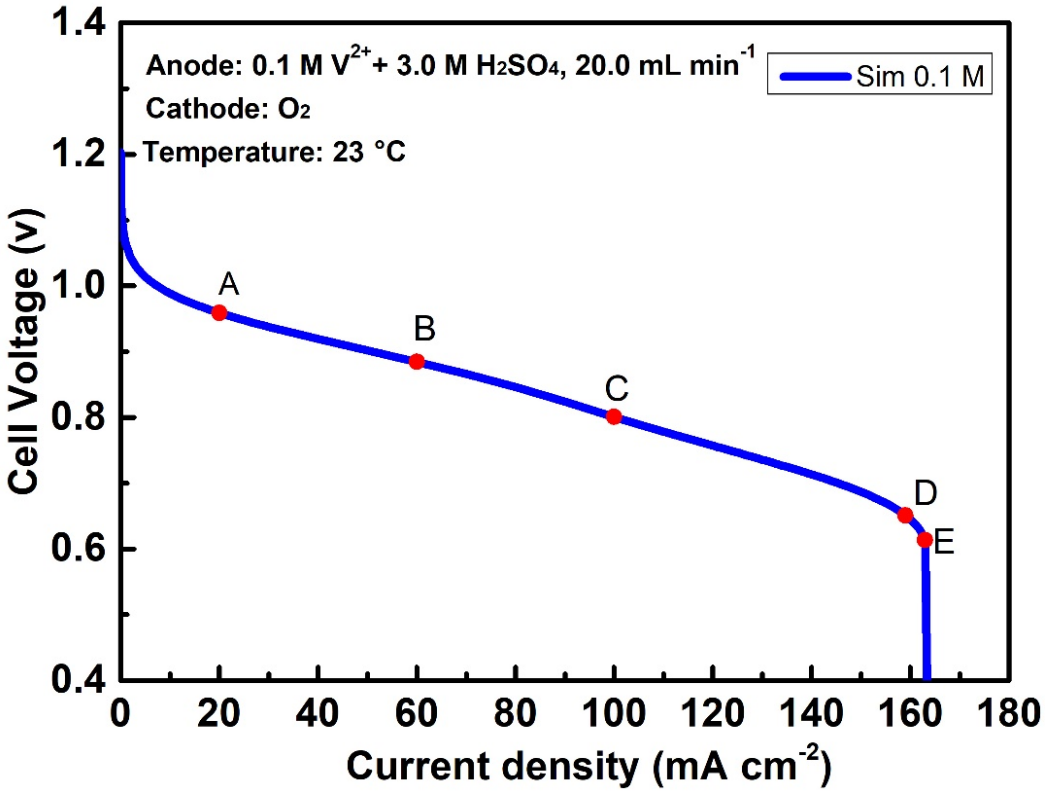

(a)

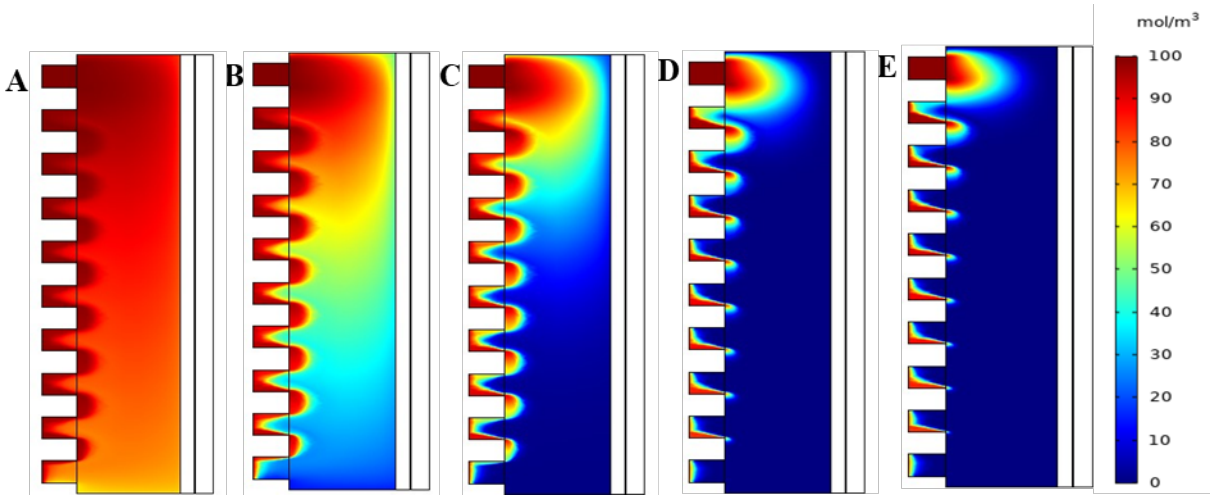

(b)

Fig. 3. (a) Polarization curve when the cell is fed with an e-fuel solution containing 0.1 M V^{2+} in 3.0 M H_2SO_4. (b) Vanadium-ion concentration distributions at designated current densities – A. 20, B. 60, C. 100, D. 160, and E. 163 mA cm^{-2}.

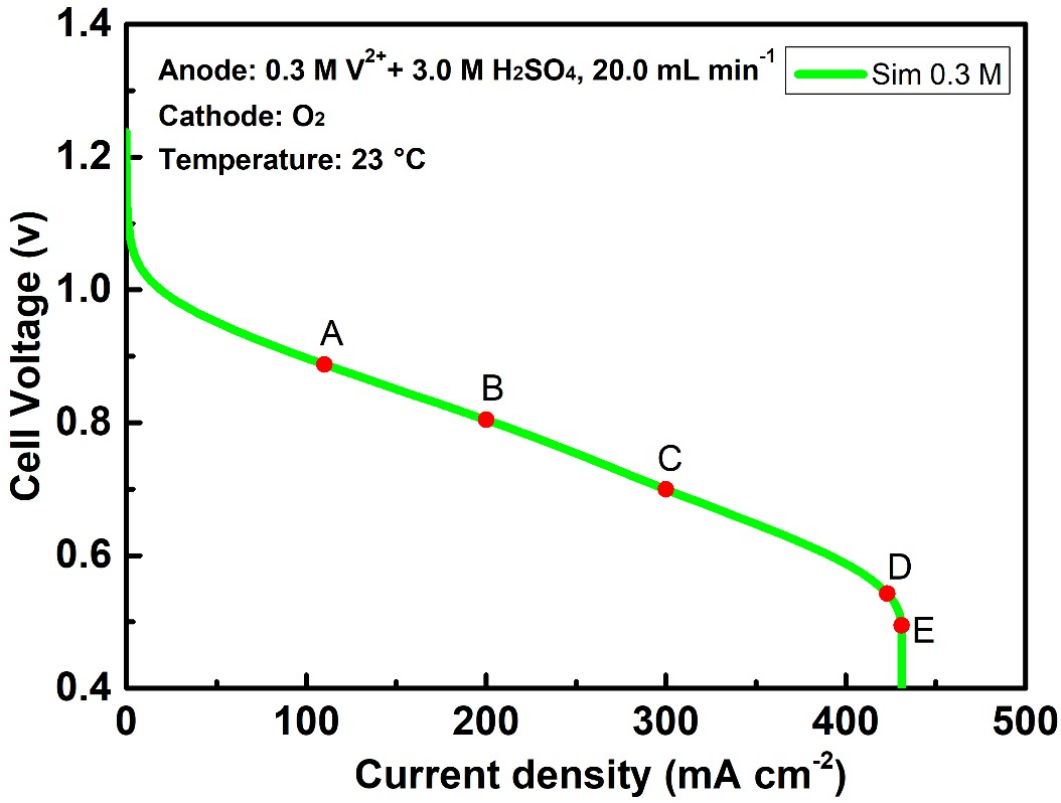

(a)

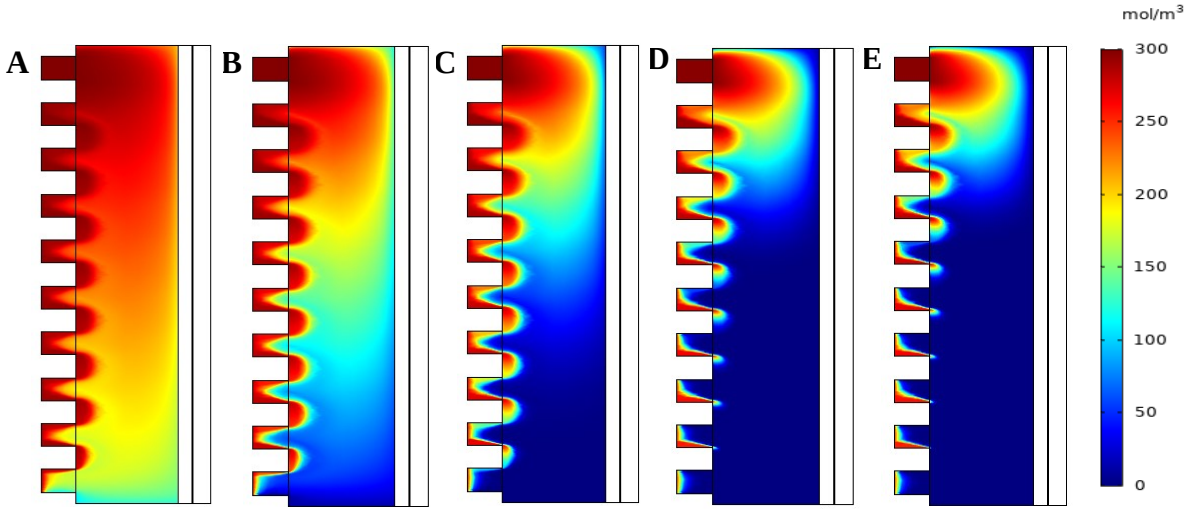

(b)

Fig. 4. (a) Polarization curve when the cell is fed with an e-fuel solution containing 0.3 M V^{2+} in 3.0 M H_2SO_4. (b) Vanadium-ion concentration distributions at designated current densities - A. 100, B. 200, C. 300, D. 423, and E. 431 mA cm^{-2}.

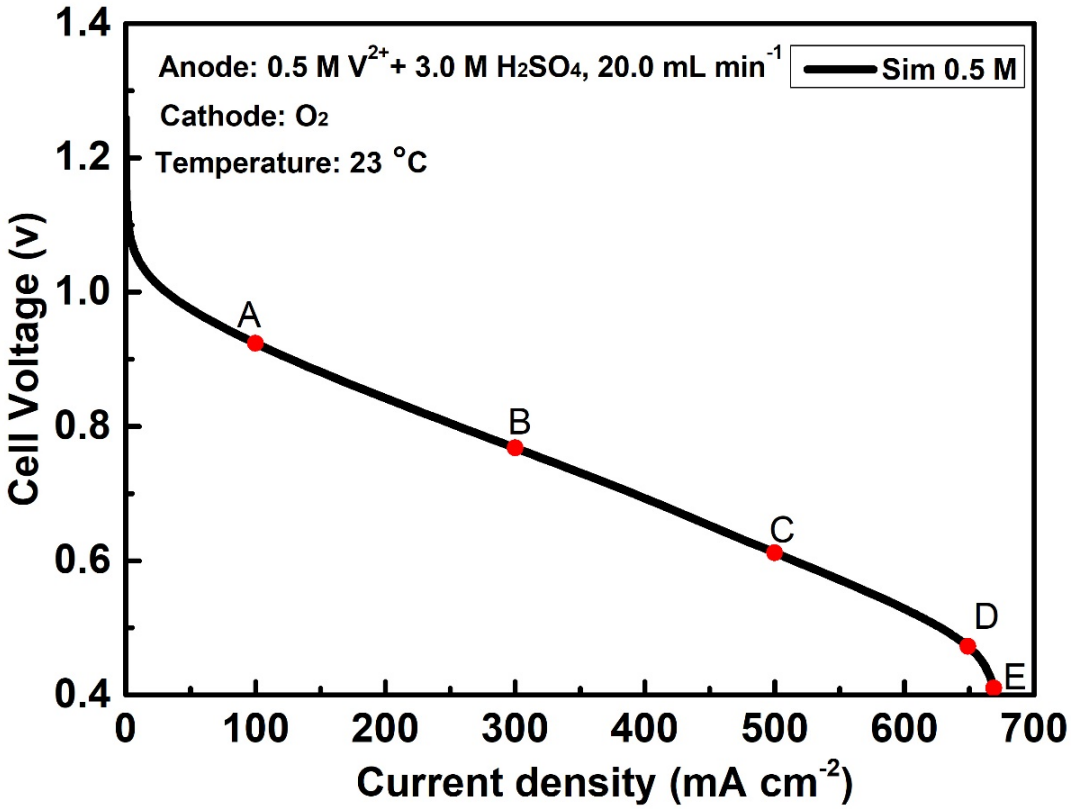

(a)

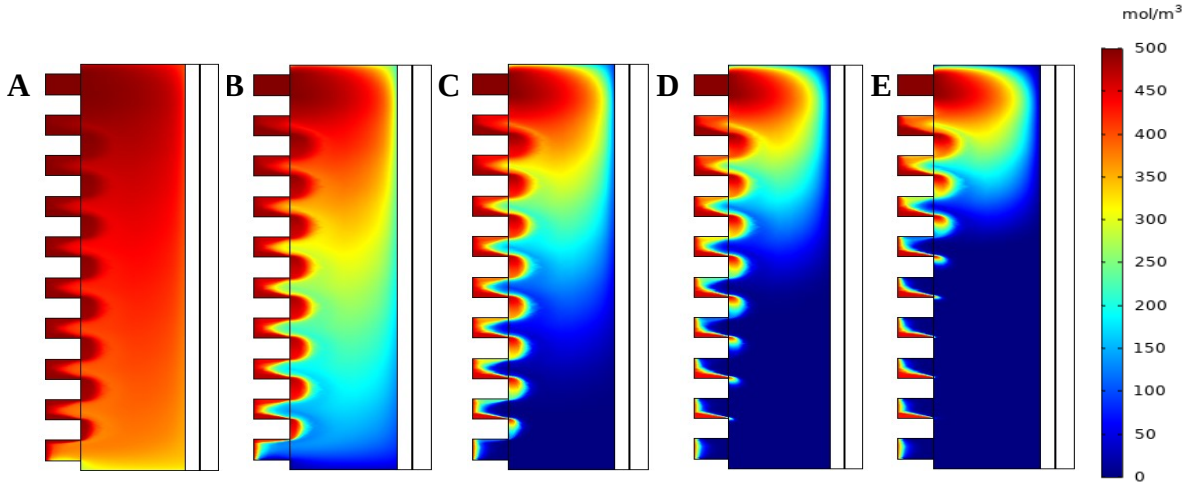

(b)

Fig. 5. (a) Polarization curve when the cell is fed with an e-fuel solution containing 0.5 M V^{2+} in 3.0 M H_2SO_4. (b) Vanadium-ion concentration distributions at designated current densities - A. 100, B. 300, C. 500, D. 650, and E. 680 mA cm^{-2}.

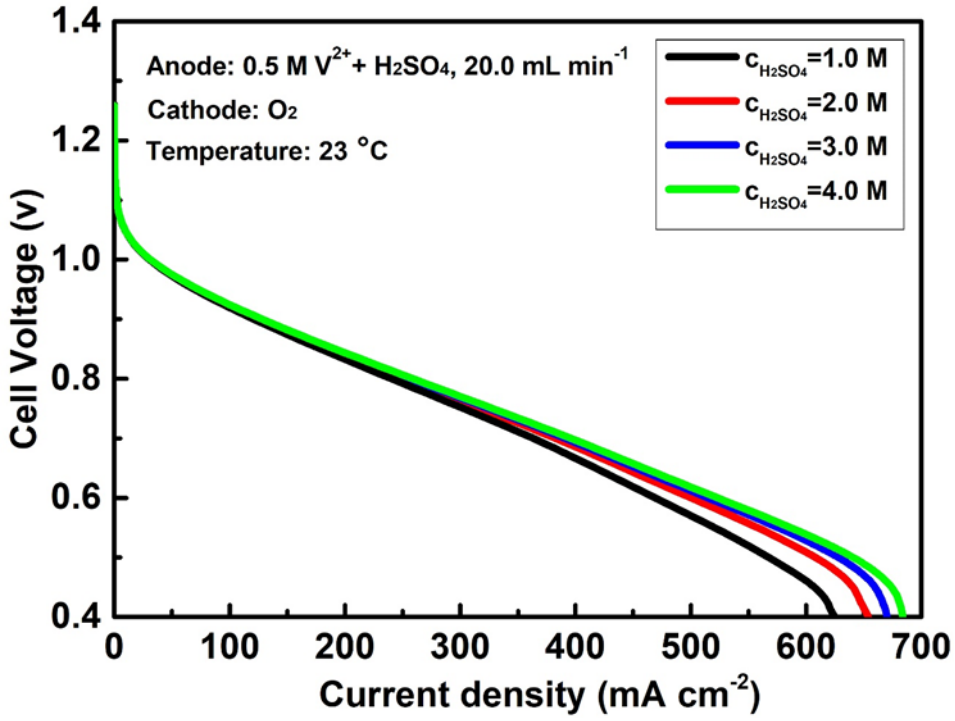

(a)

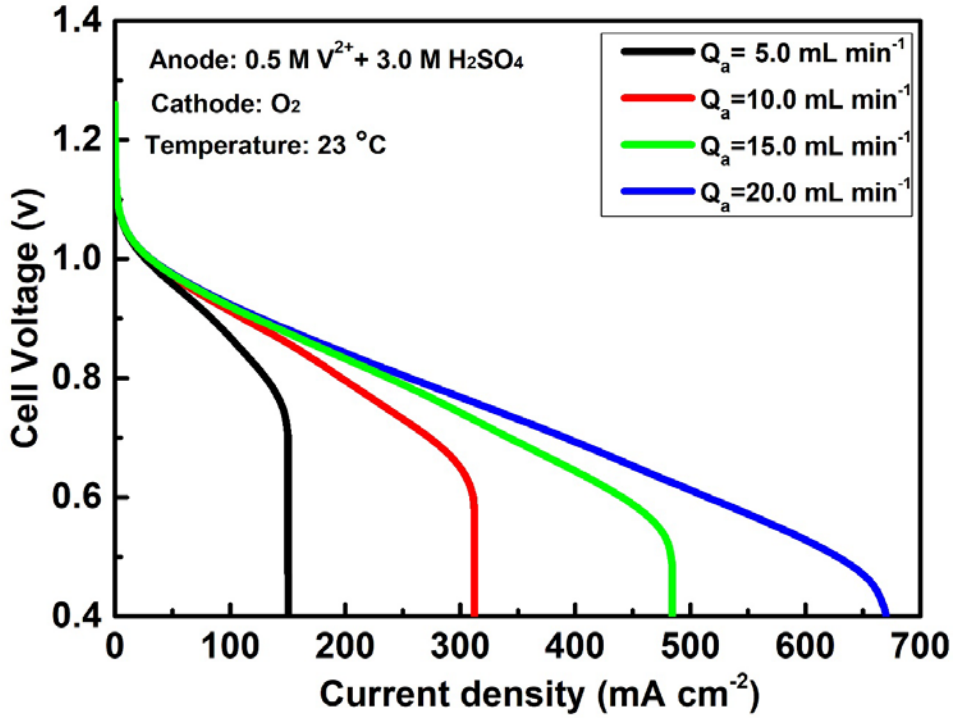

(b)

Fig. 6. Effect of the (a) sulfuric acid concentration and (b) e-fuel flow rate on the cell performance

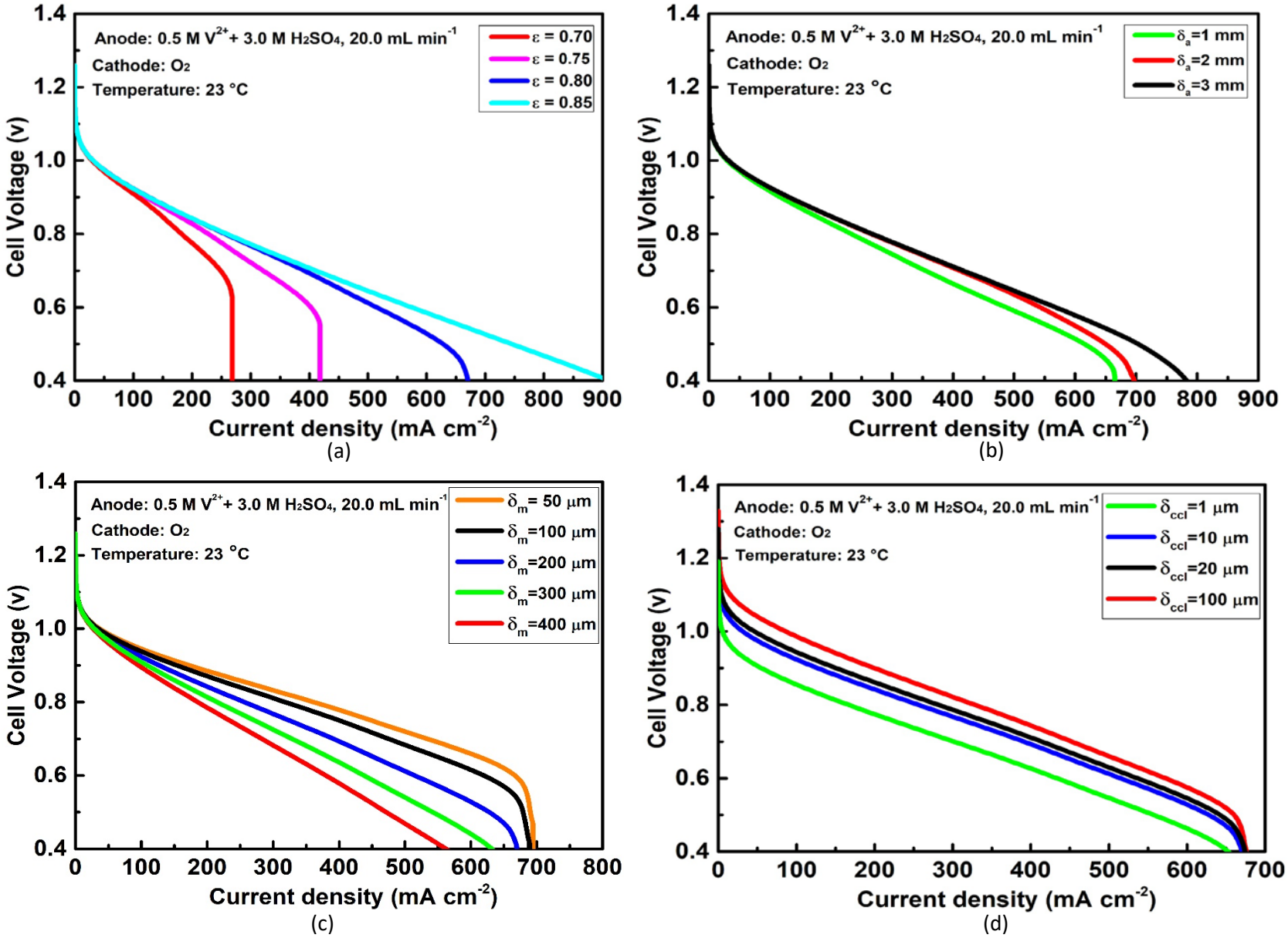

Fig. 7. Effect of the (a) anode porosity, (b) anode thickness, (c) membrane thickness, and (d) cathode catalyst layer thickness on the cell performance.

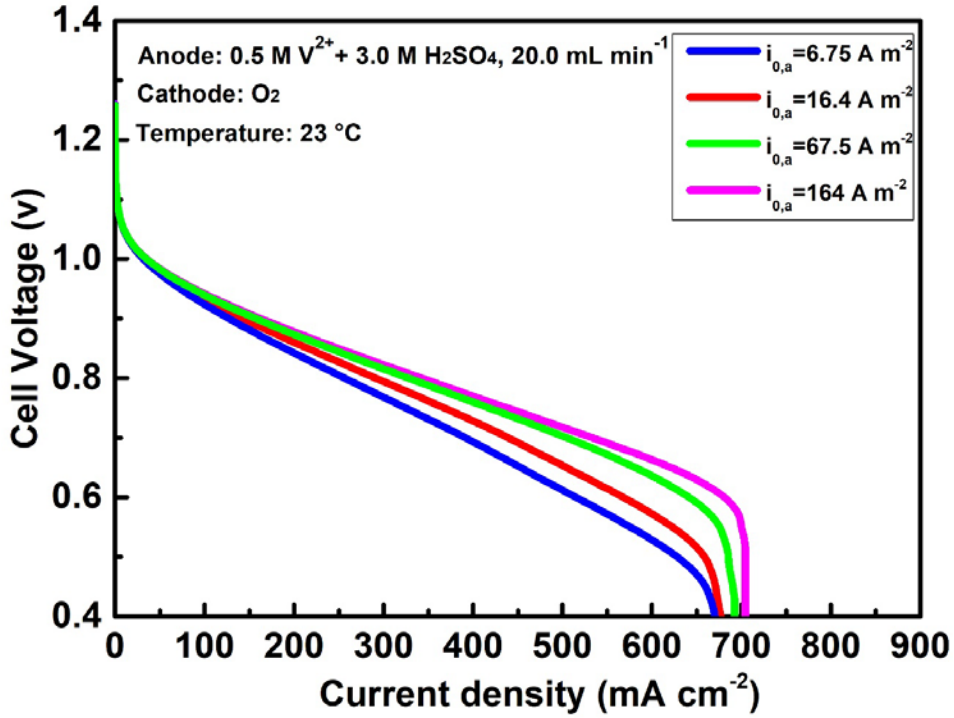

(a)

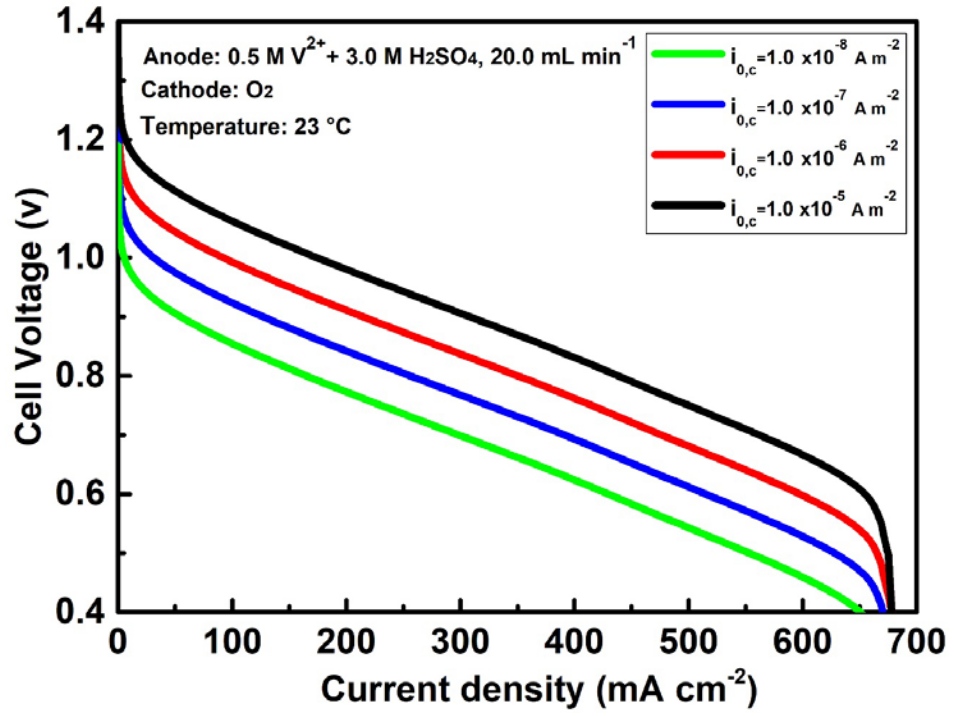

(b)

Fig. 8. Effect of the (a) anodic and (b) cathodic exchange current densities on the cell performance.

Table 1. Cell geometry properties and porous media parameters.

Symbol	Parameter description	Value	Unit	Ref.
h	Height of the cell	0.02	m	[14]
w	Width of the cell	0.02	m	[14]
$\boldsymbol{\delta_a}$	Thickness of the porous anode	0.0015	m	[14]
$\boldsymbol{\varepsilon}$	Porosity of the anode	0.8	-	[37]
d	Fibre diameter of the porous anode	10	μm	[20]
$\boldsymbol{a_a}$	Active surface area of the porous anode	3.5×10^5	m^2/m^3	[38]
A	Cross-sectional area of the flow channel	1.0×10^{-6}	m^2	[14]
$\boldsymbol{\sigma_{a,s}}$	Electrical conductivity of the porous anode	1000	S/m	[39]
$\boldsymbol{\delta_m}$	Thickness of the membrane	200	μm	[37]
$\boldsymbol{\sigma_m}$	Ionic conductivity of the membrane	7.0	S/m	[40]
$\boldsymbol{\delta_{ccl}}$	Thickness of the cathode catalyst layer	10	μm	[41]
$\boldsymbol{a_{ccl}}$	Active surface area of the cathode catalyst layer	5.6×10^7	m^{-1}	[42]
$\boldsymbol{\sigma_{c,l}}$	Proton conductivity of the cathode catalyst layer	3.05	S/m	[43]
$\boldsymbol{\sigma_{c,s}}$	Electrical conductivity of the cathode catalyst layer	2000	S/m	[44]
$\boldsymbol{\delta_{cdl}}$	Thickness of the cathode diffusion layer	260	μm	[41]

Table 2. E-fuel solution parameters and operating conditions.

Symbol	Parameter description	Value	Unit	Ref.
$c^0_{v^{2+}}$	Initial concentration of vanadium (II) ion	500	mol m^{-3}	[14]
$c^0_{v^{3+}}$	Initial concentration of vanadium (III) ion	500	mol m^{-3}	[14]
$c^0_{H^+}$	Initial proton concentration in the porous anode	6000	mol m^{-3}	[14]
μ	Viscosity of the e-fuel solution	0.005	Pa s	[21]
ρ	Density of the e-fuel solution	1680	Kg m^{-3}	[45]
T	Operating temperature	296	K	[14]
$\mathbf{Q_a}$	Volumetric flow rate of the e-fuel solution	20	mL min^{-1}	[14]

Table 3. Physicochemical parameters.

Symbol	Parameter description	Value	Unit	Ref.
k_a	Rate constant for the anodic reaction	7.0 x 10^{-8}	m s^{-1}	[23]
$\alpha_{1,a}$	Anodic charge transfer coefficient at the anode	0.5	-	[16]
$\alpha_{1,c}$	Cathodic charge transfer coefficient at the anode	0.5	-	[16]
E_a^0	Standard reduction potential of the porous anode	- 0.255	V	[16]
E_c^0	Standard reduction potential at the cathode	1.23	V	[16]
$i_{0,c}$	Cathodic exchange current density	1.0 x 10^{-7}	A m^{-2}	[40]
$\alpha_{2,c}$	Cathodic charge transfer coefficients at the cathode	0.85	-	Assumed
R	Universal gas constant	8.314	J mol^{-1} k^{-1}	
F	Faraday's constant	96 485	s A mol^{-1}	
n	Number of electrons transferred from the anode	1	-	

Table 4. Mass/charge transport parameters at the anode.

Symbol	Parameter description	Value	Unit	Ref.
$D_{V^{2+}}$	Diffusion coefficient of vanadium (II) ion	2.4 x 10^{-10}	m^2s^{-1}	[16]
$D_{V^{3+}}$	Diffusion coefficient of vanadium (III) ion	2.4 x 10^{-10}	m^2s^{-1}	[16]
D_{H^+}	Diffusion coefficient of proton	9.31 x 10^{-9}	m^2s^{-1}	[16]
$D_{SO_4^{2-}}$	Diffusion coefficient of sulphate ion	1.07 x 10^{-9}	m^2s^{-1}	[16]

Nomenclature

A	cross sectional area (m^2)
a	active surface area (m^2/m^3)
c	concentration ($mol\ m^{-3}$)
D	diffusion coefficient ($m^2 s^{-1}$)
d	diameter (m)
E^0	standard reduction potential (V)
E	potential (V)
F	Faraday's constant (s $A\ mol^{-1}$)
i	exchange current density (A m^{-2})
j	local current density (A m^{-2})
k	reaction rate constant (m s^{-1})
$\vec{N}$	molar concentration flux ($mol\ m^{-3}\ s^{-1}$)
n	number of electrons involved in the reaction
Q	flow rate (mL min^{-1})
P	pressure (Pa)
R	universal gas constant ($J\ mol^{-1}K^{-1}$)
S	source term (mol s^{-1} m^{-3})
T	operating temperature (K)
u	mobility (mol s kg^{-1})
$\vec{v}$	velocity (m s^{-1})
z	charge/valence of ion

Greek symbol

α	transfer coefficient
Ø	potential (V)
η	overpotential (V)
ρ	density ($kg\ m^{-3}$)
σ	conductivity (S m^{-1})
μ	viscosity (Pa s)
δ	thickness (m)
ε	porosity

Subscript

a	anode
c	cathode
i	species
l	liquid
s	solid
m	membrane

Superscript

eff	effective
eq	equilibrium
s	surface